Simulated three-component granular segregation in a rotating drum

D. C. Rapaport*
Physics Department, Bar-Ilan University, Ramat-Gan 52900, Israel
(Received 28 March 2007; published 19 October 2007)

Discrete particle simulations are used to model segregation in granular mixtures of three different particle species in a horizontal rotating drum. Axial band formation is observed, with medium-size particles tending to be located between alternating bands of big and small particles. Partial radial segregation also appears; it precedes the axial segregation and is characterized by an inner core region richer in small particles. Axial bands are seen to merge during the long simulation runs, leading to a coarsening of the band pattern; the relocation of particles involved in one such merging event is examined. Overall, the behavior is similar to experiment and represents a generalization of what occurs in the simpler two-component mixture.

DOI: 10.1103/PhysRevE.76.041302 PACS number(s): 45.70.Mg, 45.70.Qj, 64.75.+g, 02.70.Ns

I. INTRODUCTION

One of the more fascinating properties of granular matter is the ability of appropriately driven mixtures to separate into their individual components, despite the apparent lack of energetic or entropic advantages of an unmixed state. The segregation of a binary mixture contained in a partially filled, horizontal, rotating drum is an extensively studied problem of this class, one with obvious industrial importance. The most prominent characteristic exhibited by this system is axial segregation, in which a pattern of bands of alternating particle species forms along the cylinder axis; the bands merge and the pattern coarsens over time, at a rate that drops to such a low level that it is unknown whether the state eventually reached is stable, or merely long-lived. A second form of segregation, though one that can require greater effort to observe, occurs in the radial direction, producing a core rich in small particles surrounded by an outer layer of mainly big particles; this core can either be a transient on the path to later axial segregation, or a feature that persists even when full axial segregation is apparent from external views.

In the case of mixtures of two species, early experimental efforts involved direct observation of the axial band structure at the outer surface [1], whereas some of the subsequent studies succeeded in examining the interior using MRI [2,3] and relating the development of the axial bands to bulges occurring in the radial core. Time-dependent behavior can occur subsequent to the initial appearance of the axial bands; narrower bands gradually merge to form broader bands [4] and traveling surface waves have been noted [5]. Complicating the behavior are results showing that the ratio of cylinder to particle diameter determines if axial segregation can occur and whether its appearance depends reversibly on rotation rate [6]. Further recent experimental examples [7,8] reveal more about the richness of the segregation effect and the associated dynamics under wet conditions; these are relevant because the behavior of slurries tends to be similar to dry mixtures. Overall, no consensus has yet emerged as to the nature of the mechanisms underlying this complex set of segregation phenomena. For further discussion of the difficulties inherent in understanding granular matter in general see, e.g., Refs. [9–11].

In contrast to the many studies involving two-component systems (only a selection of which were cited above), three-component systems have received far less attention. The experimental results available for systems with three particle species [12] were obtained using glass beads of different sizes (an earlier brief discussion appears in Ref. [13]). The description of the experiment relates that, after beginning with an initially uniform mixture, the first effect to occur is the appearance of radial segregation, in which there is an inner core of small particles and an outer layer of big particles, with the medium-size particles lying predominantly in between. This is followed by the development of axial bands of medium-size particles in the mainly big-particle outer region, followed by the appearance of small-particle bands within the medium-particle bands. Replacing the opaque big and/or medium particles with transparent equivalents reveals that the small-particle core persists after the onset of axial segregation, and that a layer of medium-size particles surrounds it. Systems with more than three components are also mentioned, with four components showing behavior analogous to three, while beyond four the axial segregation is no longer seen, but these lie outside the scope of the present work. As with two-component systems, the behavior is certain to be influenced by the relative species sizes and concentrations, as well as by the many parameters required to fully specify the system, including the fill level, frictional properties, and rotation speed, although their influence on the nature of the segregation is not described.

Simulations of granular systems based on discrete-particle models have proved capable of reproducing both the axial and radial forms of segregation, in qualitative agreement with experiment. The present paper extends an earlier study [14], in which two-component systems were modeled. In that paper it was shown how the appearance of radial segregation preceded axial segregation, and that depending on the circumstances, a radial core of small particles could still be present even after the exterior view showed essentially complete axial segregation. Owing to the need for long runs and large systems, only a limited set of parameter combinations could be considered. The problem of following the development of segregation in detail is further exacerbated by a lack of reproducibility between runs differing only in the random

*rapaport@mail.biu.ac.il

velocities assigned to the particles in the initial state that result in different segregation scenarios. While similar effects occur experimentally, the implication is that multiple simulation runs are essential to ensure that the "typical" behavior is captured. In view of the potentially heavy computational demands, a thorough study of the two-component system and a detailed comparison with the variety of experimental data available has yet to be undertaken.

The obvious next stage in this exploration is to increase the number of granular species, and while this has been carried out experimentally, as indicated above, the corresponding simulations have yet to be carried out. The goal of the present paper, therefore, is to demonstrate that the model used previously is also able to produce the appropriate kinds of segregation even when three species are involved. Given the very limited amount of experimental information presently available for this problem, any systematic coverage of the parameter space is premature; the discussion is therefore confined to specific examples illustrating the main features of simulated three-component segregation.

II. METHODOLOGY

The granular model employs spherical particles whose overlap repulsion is based on a continuous potential [15–17], exactly as in [14]. The normal force between a pair of particles (i,j) includes a repulsion that depends linearly on the overlap and a velocity-dependent damping force

$$\boldsymbol{f}_n = [k_n(d_{ij} - r_{ij}) - \gamma_n(\hat{\boldsymbol{r}}_{ij} \cdot \boldsymbol{v}_{ij})]\hat{\boldsymbol{r}}_{ij}, \quad r_{ij} < d_{ij}, \tag{1}$$

where $\boldsymbol{r}_{ij}$ and $\boldsymbol{v}_{ij}$ are the particle separation and relative velocity, and $d_{ij}=(d_i+d_j)/2$ is the mean diameter. The two parameters appearing in Eq. (1), k_n governing the stiffness and γ_n the normal damping, are the same for all particles.

Sliding of particles that are within interaction range is opposed by both frictional damping and a transverse restoring force

$$\boldsymbol{f}_t = -\gamma_s^{c_i c_j}\boldsymbol{v}_{ij}^s - k_g\int_{(\mathrm{coll})} \boldsymbol{v}_{ij}^s(\tau)d\tau, \tag{2}$$

where $\boldsymbol{v}_{ij}^s$ is the relative transverse velocity allowing for particle rotation, and the integral is evaluated as the sum of vector displacements over the collision period (additionally, whenever the integrated displacement exceeds 0.1 it is reset to zero). The magnitudes of both terms in Eq. (2) are bounded by $\mu^{c_i c_j}|\boldsymbol{f}_n|$. The transverse damping and static friction coefficients, $\gamma_s^{c_i c_j}$ and $\mu^{c_i c_j}$, depend on the particle types c_i and c_j; the transverse stiffness k_g is the same for all particles.

The majority of parameter settings are taken from [14] and, as before, the curved cylinder wall and the flat end plates are treated as rough and smooth boundaries, respectively. The value of the gravitational acceleration, $g=5$, relates the dimensionless molecular dynamics (MD) units of the simulation to the corresponding physical units. If L_{MD} is the length unit (in mm), then the time unit is $T_{\mathrm{MD}} \approx 10^{-2}\sqrt{5L_{\mathrm{MD}}}$ s. A cylinder rotating with angular velocity Ω (MD units) has an actual rotation rate of $\Omega/(2\pi T_{\mathrm{MD}}) \approx 7.1\Omega/\sqrt{L_{\mathrm{MD}}}$ Hz; for 4 mm particles, $\Omega=0.2$ is equivalent to an experimental 43 rpm. Other details of the simulations are covered in Ref. [18], and the required MD techniques are described in Ref. [19].

Efficiently evaluating the displacement sums in Eq. (2) requires maintaining a list of all currently interacting particle pairs in a form that is readily accessible given the identity of the pair involved, but also easily modified as pairs are added or deleted due to the continually changing identities of interacting neighbors. Of the approaches available for organizing the data, the one used here (as well as in Ref. [14], although the description was omitted) is the following.

A table is constructed that holds a set of linked lists of interacting pairs (i,j), ordered so that $i<j$. Each entry consists of the value of j, a pointer to another entry used to link entries with a common i, the current value of $\boldsymbol{u}_{ij} = \Sigma_{(\mathrm{coll})}\boldsymbol{v}_{ij}^s(\tau)$ needed in Eq. (2), and the time step number t_{ij} at which $\boldsymbol{u}_{ij}$ was last updated. There is a separate list for each particle i, and a pointer h_i to the first entry in its list; from h_i the list can be scanned using the pointers to obtain all interacting neighbors with $j>i$, until a null pointer ends the list. For each interacting pair encountered during the force calculations, the corresponding $\boldsymbol{u}_{ij}$ and t_{ij} are updated; new entries are readily added as necessary, whereas if a previously interacting pair is no longer in range its entry will not be updated. After all the forces have been evaluated, those entries whose t_{ij} are not current (because $r_{ij}>d_{ij}$) have their $\boldsymbol{u}_{ij}$ reset to zero. Expired entries need not be deleted immediately since pairs are capable of moving in and out of range many times, in which case, if the relevant entry is still in the table it will be reused. (On a shared-memory computer, if the neighbor list references the relevant table entries, the force computations can be carried out in parallel [19], even with this history-dependent interaction.)

The force parameters are $k_n=1000$, $\gamma_n=5$, and $k_g=500$. Transverse damping (or dynamic friction) depends on particle type; if b, m, and s denote big, medium, and small sizes, then $\gamma_s^{bb}=10$, $\gamma_s^{mm}=6$, $\gamma_s^{ss}=2$, and the lower of the values is used for unlike species (the bb and ss values are from Ref. [14], and the mm value is their mean). Finally, the relative values of the static friction coefficients, e.g., μ^{bb}/μ^{ss}, are set equal to the ratio of the corresponding γ_s values, with the larger of the pair equal to 0.5. In general, there seems to be considerable latitude in choosing the parameter settings, and what is required at this exploratory stage is the ability to produce results that are qualitatively reasonable.

The nominal particle diameters correspond to the interaction cutoff. As in Ref. [14], for small particles $d_s=2^{1/6} \approx 1.122$ (MD units). For big particles $d_b=2d_s$, and for medium particles $d_m=1.3d_s$; this choice of relative sizes is not too different from that used experimentally. The actual small-particle diameters are uniformly distributed over a narrow range $[d_s-0.2,d_s]$ (the mean diameter of the small particles is then close to unity), and likewise for the other species. Particles all have the same material density.

III. RESULTS

Three simulation runs are singled out for analysis here, each aimed at demonstrating particular features of the behav-

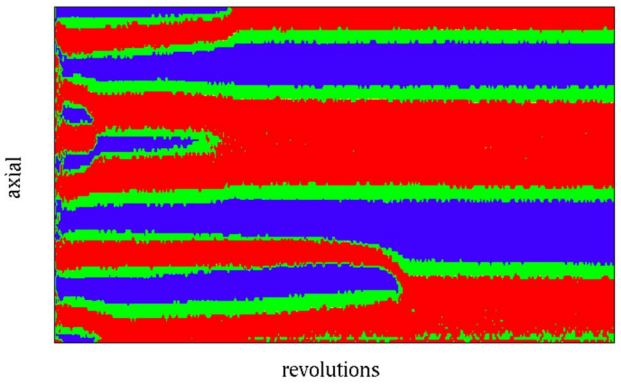

FIG. 1. (Color online) Axial space-time plot for run #A ($L=240$, $L/D=8$, $n_R=4260$); red, green, and blue (or medium, light, and dark shades of gray) denote whether the big, medium, or small particles have the highest volume fraction. Time is along the horizontal axis, and the vertical axis corresponds to axial position.

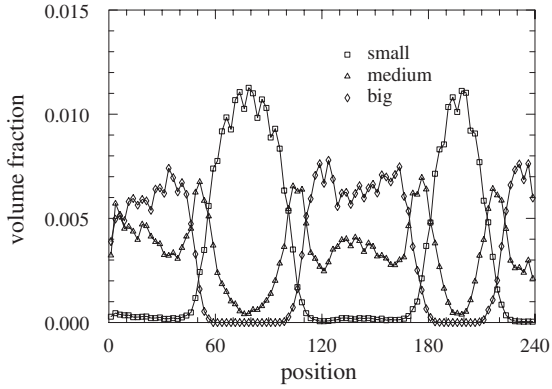

FIG. 2. Volume fractions of the three particle species measured in slices normal to the axis for the axially segregated state near the end of run #A (distance is expressed in dimensionless MD units).

ior. They employ cylinders with diameter $D=30$ or 40 (reduced units) that are rotated with angular velocity $\omega=0.2$ where particle flow is continuous; these are the values used for the majority of runs in the two-component study [14]. Runs are begun with the particles arranged on a lattice at a specified density (this determines the eventual fill level) and assigned random velocities. Particle species are assigned randomly, producing an initially mixed state; the relative populations of the three kinds of particles are chosen to ensure equal volume fractions of all species.

The first of the runs #A involves a cylinder of length $L=240$ and diameter $D=30$ (aspect ratio $L/D=8$); the initial filling density is $\rho=0.25$, resulting in a system with $N=29\,704$ particles. The total run length is $n_R=4260$ revolutions, and the purpose of this comparatively long run (by simulation standards) is to demonstrate the ability to produce an apparently stable axial band pattern after the effects of the initial transients have disappeared. The second run #B employs a longer cylinder, $L=360$, with the same D and filling density, so that $N=44\,556$; the run length $n_R=2300$ is shorter, and the higher aspect ratio (=12) can accommodate a more extensive set of axial bands. In the third run #C the cylinder length is reduced to $L=120$, the diameter increased to $D=40$, and the fill level raised by setting the initial density to $\rho=0.4$ so that $N=47\,520$; this is a shorter run whose goal is to provide increased space for observing the development of radial segregation.

The behavior encountered in each of these runs is described in detail below. This is accomplished using a combination of axial space-time plots that summarize the overall development of axial segregation, graphs showing the concentrations of each of the particle species along the axial and radial directions, and images of individual configurations that reveal where particles actually reside.

Figure 1 shows the axial space-time plot for run #A. In view of the need to distinguish between three species, rather than just two, the color coding shows only the volume-weighted majority species, irrespective of the degree to which the other species might be present; in this respect the present space-time plots differ from Ref. [14] where a continuous color gradient designates the relative volume fraction itself. The plot shows that during slightly over half of the run a series of band merging events occurs, most within the first 1200 revolutions and the last at approximately 2500, eventually producing a state with 10 axial bands (counting all species, where one of the end bands is only weakly defined), and there is no apparent change thereafter. While the possibility of future change cannot be excluded, none was observed when the run was subsequently extended by an extra 1000 revolutions (not shown). The rapid, small fluctuations at the band boundaries are artifacts of the discrete nature of the majority rule by which color is determined.

More detailed information concerning the band occupancy at the end of run #A appears in Fig. 2. The plot shows the volume fractions of each of the particle species in a sequence of slices oriented normal to the cylinder axis; fluctuations in the measurements are reduced by averaging over ten successive configurations, sampled once per revolution. It is clear that the b and s particles are well segregated axially. On the other hand, the axial separation of m and b particles is less pronounced than for m and s; while the m particles exhibit a distinct preference for the regions located between b and s bands, and their occupancy drops to a very low level in the middle of the s bands, they are seen to maintain a significant minority presence throughout the b bands.

Adding an extra time dimension to Fig. 2 provides a more detailed description of the segregation process than is available in the space-time plot, but the results for the three species must be graphed separately to ensure the features are visible. The time-dependent distribution of small particles is displayed as a surface plot in Fig. 3; prominent features include the emergence of the peaks in the axial distribution and the subsequent peak changes corresponding to axial band reorganization.

Figure 4 shows the volume fractions at an early stage of run #A (after approximately 37 revolutions, prior to the appearance of any axial effects) in a manner aimed at revealing the presence of radial segregation. In order to achieve this, the system is divided into a series of slices that are oriented parallel to the mean direction of the upper free surface of the mixture (as in Ref. [14], the slope is determined by a linear

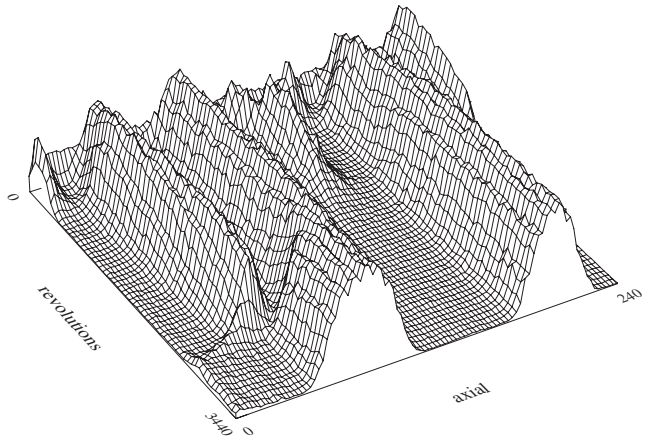

FIG. 3. Development of the peaks in the axial distribution of small particles for run *#A*.

fit to the inner 2/3 of the surface away from the curved boundary) and the relative volume fractions in the slices evaluated (also limited to a region of the same width to avoid bias); the results are again averaged over ten configurations, at one-revolution intervals, for improved statistics. The *b* and *s* particles are seen to experience a certain degree of radial segregation, with *s* dominating the interior and *b* on the outside, but the *m* particles exhibit no radial preference (the behavior is slightly different in run *#C*, below, where the particle layer has double the maximum thickness due to larger *D* and a higher fill level).

Figure 5 shows the axial space-time plot for run *#B*, where the longer cylinder allows the formation of a greater number of axial bands. Several band merging events are apparent, most during the first 400 revolutions and the last at about 1200, resulting in 19 bands at the end of the run; the final band merge will be examined in greater detail below. A plot of the volume fractions as a function of axial position at the end of the run is shown in Fig. 6; once again the *b* and *s* particles are well segregated, while the *m* particles exhibit the same preference for the regions between the *b* and *s* bands and a minority presence inside the *b* bands, as in run *#A*.

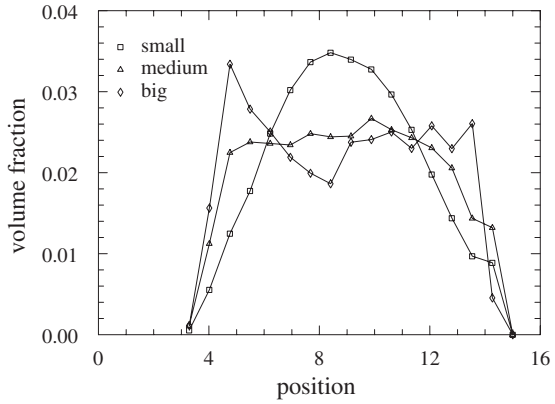

FIG. 4. Volume fractions of the particle species early in run *#A* measured in slices parallel to the free surface (the cylinder axis is at the origin).

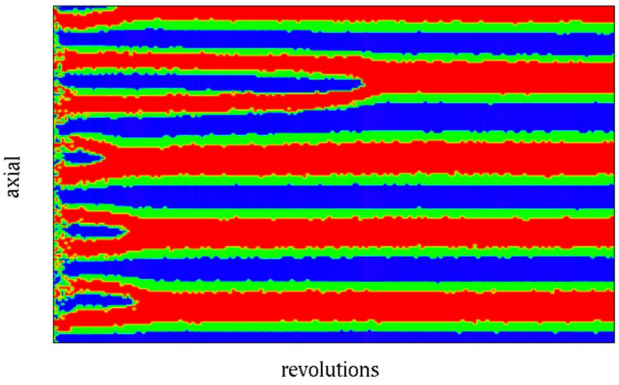

FIG. 5. (Color online) Axial space-time plot for run *#B* ($L=360$, $L/D=12$, $n_R=2300$).

While the colored space-time plots only allocate a single column of pixels to describe the state of the entire system at each instant, images of the evolving patterns viewed from above provide a more detailed history resembling what would be seen experimentally. Figure 7 shows the state of run *#B* after approximately 20, 60, 100, 200, 400, 800, and 1600 revolutions; the images cover the early portion of the run where there is no hint of axial segregation (although there are radial processes occurring beneath the surface), followed by the pattern coarsening stage, and the steady state that persists throughout the latter part of the run.

Figure 8 contains views of the final state of run *#B* as seen from the outside, along with images of the individual species that correspond to what might be observed experimentally, either using MRI, or by replacing any two of the species with transparent particles having similar mechanical properties. The first two views are of the system seen from above and below (the view direction is approximately normal to the free surface); the remaining views each show a single particle species. The *b* and *s* particles are seen to occupy well-defined axial bands; the *m* particles, however, show only partial axial segregation, an observation confirmed quantitatively in Fig. 6. A feature apparent from the pictures is that the boundaries of the *b* and *s* bands are not vertical, with the *s* bands being narrower at the upper free surface.

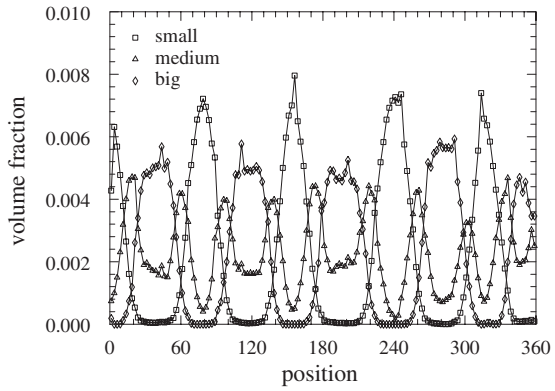

FIG. 6. Volume fractions of the particle species in the axially segregated state near the end of run *#B*.

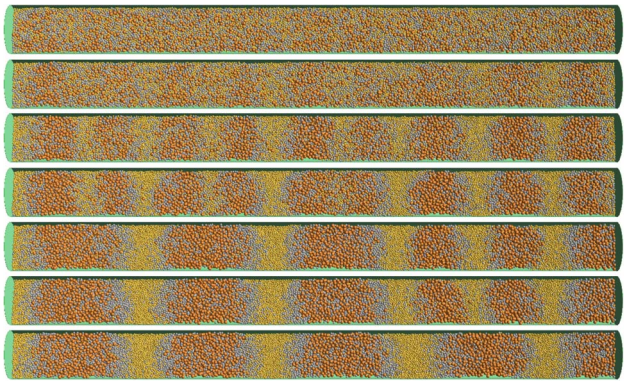

FIG. 7. (Color online) Surface views of run *#B* at different times.

The distribution of volume fractions for run *#C* after 35 revolutions, evaluated as before to demonstrate the presence of radial segregation (also averaged over ten configurations), is shown in Fig. 9. Unlike the case of run *#A* earlier, the behavior is more clearly resolved due to the larger cylinder diameter and higher fill level. There is now also a suggestion of the *m* particles having preferred radial positions, although the effect is still much weaker than for the *b* and *s* particles. A view showing three slices cut out of the system appears in Fig. 10; what can be seen here reinforces the conclusion from Fig. 9, that despite the noise, the *b* and *s* particles show distinct preferences for the exterior and interior, respectively, with the *m* particles also preferentially located toward the exterior, though to a lesser degree than *b* (axial segregation begins later in this run, although the low aspect ratio impedes its development).

When comparing the simulation results with experiment, apart from any possible shortcomings of the model, allowance must be made for the relatively small system sizes that can affect the results. Given that the computational requirements depend on the product of N and n_R, the need to avoid excessively long simulations means that the ratio of cylinder diameter to particle size D/d_s must be smaller than in experiment; in addition to finite-size effects in general, this particular limitation has been shown to influence behavior experimentally [6]. Nevertheless, to the extent that it is possible to compare the three-component simulations with the limited experimental data available [12], the similarity is encouraging, in particular, the organization of the axial bands, with the bands of *m* particles located between alternating *b* and *s* bands. The fact that experiment indicates that a core of *m* particles persists within the *b* bands is also in agreement with the simulations, even if in the latter the core is less well defined.

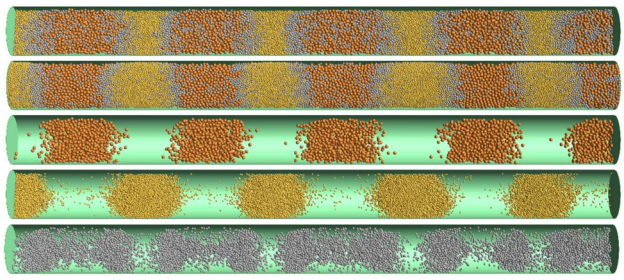

FIG. 8. (Color online) Final state of run *#B*; the full system seen from above and below, and separate views of the big, small and medium size particles, colored copper, gold and silver, respectively.

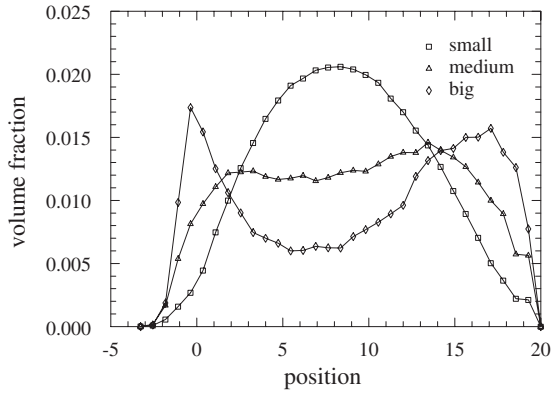

FIG. 9. Volume fractions of each particle species early in run *#C* measured in slices parallel to the free surface (the cylinder axis is at the origin).

As always, however, it is the deviations from experiment that must be considered. For example, experiment suggests that, in addition to the axial *m* bands being more sharply defined, there is apparently an innermost core of *s* particles (surrounded by *m* particles). Whether such differences, in particular the latter, are due to basic flaws in the model, or whether they are merely consequences of a less than ideal parameter choice (perhaps as simple as the range of particle sizes), or too narrow a cylinder, must await future study, both simulational and experimental.

The final example considered involves the band merging event of run *#B* that occurs between revolutions 700 and 1450 at a location in the cylinder sufficiently far from the end plates to be free from any interference. An analogous study was carried out for the two-species system [14], but with three species the details are more complex. Figure 11 shows what becomes of the occupants of the merging *b*

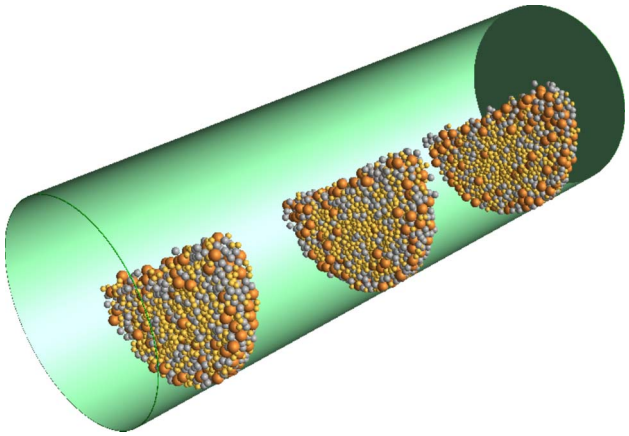

FIG. 10. (Color online) Run *#C* after 35 revolutions; three narrow slices through the system are shown.

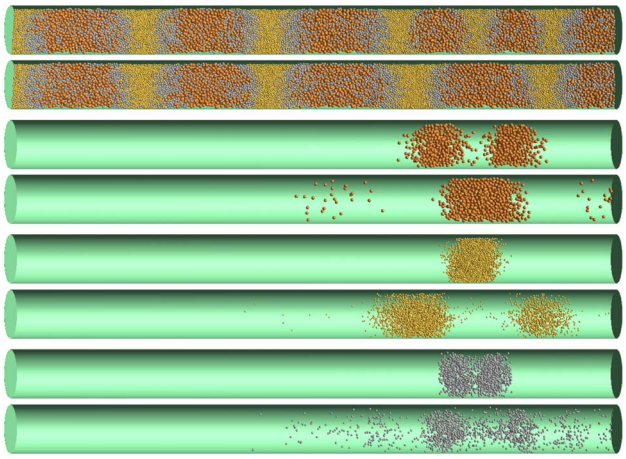

FIG. 11. (Color online) Band merging in run *#B*; the views show the full system and the individual particles from the *b*, *s*, and *m* bands involved (only the inner portions of the *m* bands), both before and after the event.

bands and the vanishing *s* and *m* bands. The first two images are of the entire system seen from above, before and after the event; pattern changes are limited to the neighborhood of the merging bands. Each subsequent pair of images shows the particles of a single species within the affected bands, both before the event (including particles beneath the surface intruding into adjacent bands) and afterward; in the case of the *m* particles, only those initially in the inner halves of the two bands are considered. The *b* bands are seen to merge with only the slightest scatter outside the newly formed band. The *s* band disperses into the adjacent bands with practically no scatter beyond the bands receiving these particles. In the case of the *m* bands (where only the inner half bands are tracked) the contents are seen to disperse to a greater degree than the *b* bands; such behavior is consistent with the fact that axial segregation, and hence confinement, is weakest for the *m* particles.

IV. CONCLUSION

Particle-based simulations of three-component granular systems in a rotating drum have been used in demonstrating that both axial and radial segregation can be produced using a simple model for the granular particles and their interactions. In the case of the two-component systems considered previously, there was already a relatively large set of parameters whose settings are potentially capable of influencing the behavior; with three components the set is even larger. Exploring the consequences of systematic parameter variations on the behavior, and developing a closer connection between simulation and experiment, are subjects for future study.

[1] O. Zik, D. Levine, S. G. Lipson, S. Shtrikman, and J. Stavans, Phys. Rev. Lett. **73**, 644 (1994).
[2] K. M. Hill, A. Caprihan, and J. Kakalios, Phys. Rev. E **56**, 4386 (1997).
[3] M. Nakagawa, S. A. Altobelli, A. Caprihan, and E. Fukushima, Chem. Eng. Sci. **52**, 4423 (1997).
[4] V. Frette and J. Stavans, Phys. Rev. E **56**, 6981 (1997).
[5] K. Choo, M. W. Baker, T. C. A. Molteno, and S. W. Morris, Phys. Rev. E **58**, 6115 (1998).
[6] A. Alexander, F. J. Muzzio, and T. Shinbrot, Granular Matter **5**, 171 (2004).
[7] T. Arndt, T. Siegmann-Hegerfeld, S. J. Fiedor, J. M. Ottino, and R. M. Lueptow, Phys. Rev. E **71**, 011306 (2005).
[8] T. Finger, A. Voigt, J. Stadler, H. G. Niessen, L. Naji, and R. Stannarius, Phys. Rev. E **74**, 031312 (2006).
[9] H. M. Jaeger, S. R. Nagel, and R. P. Behringer, Rev. Mod. Phys. **68**, 1259 (1996).
[10] L. P. Kadanoff, Rev. Mod. Phys. **71**, 435 (1999).
[11] I. S. Aranson and L. S. Tsimring, Rev. Mod. Phys. **78**, 641 (2006).
[12] M. Newey, J. Ozik, S. M. van der Meer, E. Ott, and W. Losert, Europhys. Lett. **66**, 205 (2004).
[13] S. D. Gupta, D. V. Khakhar, and S. K. Bhatia, Chem. Eng. Sci. **46**, 1513 (1991).
[14] D. C. Rapaport, Phys. Rev. E **75**, 031301 (2007).
[15] P. A. Cundall and O. D. L. Strack, Geotechnique **29**, 47 (1979).
[16] O. R. Walton, in *Mechanics of Granular Materials*, edited by J. T. Jenkins and M. Satake (Elsevier, Amsterdam, 1983), p. 327.
[17] P. K. Haff and B. T. Werner, Powder Technol. **48**, 239 (1986).
[18] D. C. Rapaport, Phys. Rev. E **65**, 061306 (2002).
[19] D. C. Rapaport, *The Art of Molecular Dynamics Simulation*, 2nd ed. (Cambridge University Press, Cambridge, 2004).